Transport and dispersion in random networks with percolation disorder

J. Koplik
Schlumberger-Doll Research, Ridgefield, Connecticut 06877-4108

S. Redner
Center for Polymer Studies and Department of Physics, Boston University, Boston, Massachusetts 02215

D. Wilkinson
Schlumberger-Doll Research, Ridgefield, Connecticut 06877-4108

(Received 28 May 1987)

The transport of dynamically neutral tracer in flow through a random network of tubes with percolation disorder is investigated. For each bond of the system, the tracer motion is governed by a convection-diffusion equation, with the drift term accounting for the local bond velocity. This represents an extension of random walks in disordered media to the important case of finite macroscopic flow rates. A calculational technique is developed which provides, for a given configuration of the disorder, the *exact* moments of the distribution of transit times for the tracer to traverse the system. This approach is implemented numerically for $L \times L$ random networks at the bond percolation threshold. When the total fluid flux Q vanishes, the kth moment of the transit time is found to scale with sample size as $L^{k(2+\theta)}$, where $\theta = t - \beta/\nu$ is the exponent describing the scale dependence of the diffusion coefficient of the "ant in the labyrinth," $D_{\rm ant}$. By contrast, when Q becomes large, the kth moment is found to scale as $Q^{-1}L^{2-\beta/\nu+(k-1)(2+\theta)}$. This behavior of the moments at large Q is explained on the basis of a simple heuristic argument and from a more detailed analytical calculation. Furthermore, a scaling ansatz for the transit-time moments is postulated which describes our data for all flow rates. The large-Q behavior of the moments leads to a longitudinal dispersion coefficient which scales as $U^2L^2/D_{\rm ant}$, where U is the average flow velocity, in agreement with a prediction of de Gennes.

I. INTRODUCTION

A fundamental question in flow through porous media is the nature of the transport of dynamically neutral tracer when it is injected into a fluid flowing in a porous medium.[1-3] Of particular experimental relevance is the average time needed for the tracer to traverse a given distance, and also the rate of spread of a localized pulse of tracer when carried in a steady-state flow. The former process provides information about the permeability of the medium, while the latter process, known as hydrodynamic dispersion, yields more detailed structural information. For a relatively homogeneous system, a localized tracer pulse asymptotically evolves to a Gaussian distribution whose variance grows linearly in time, multiplied by a proportionality constant that is known as the longitudinal dispersion coefficient, $D_{\parallel}$. Most previous work on transport in random media has primarily considered the two properties discussed above, which involve only the first two moments of the distribution of times for the tracer to traverse a given length in the system. (See, e.g., Refs. 4 and 5, and for a notable exception see Ref. 6.)

More generally, one may consider the full distribution of transit times and study scaling properties of arbitrary moments, in order to obtain a better understanding of flow in porous media. In this paper, we study the properties of this distribution in the case of flow occurring in a poorly connected porous medium. We focus our attention on percolation disorder,[7] in which the medium consists of a lattice network of identical tubes which are either present (with probability p) or absent (with probability $1-p$). This type of disorder should be of relevance for the situation where dispersion is taking place in one of two immiscible fluids present in a porous medium, since it is often the case that the configurations adopted by the two fluids are determined by percolation mechanisms.[8-10] In our network model, the flow in each tube is determined by the local pressure drop across it upon the imposition of a given value of the external pressure drop across the system. This flow is essentially the same as the current flow in each bond for a corresponding random resistor network with an appropriately chosen value of the external potential drop.

In the presence of this steady-state background flow, we have calculated the detailed microscopic rules which govern the motion of the tracer at the level of single tubes and tube junctions. These rules follow from a "perfect mixing" assumption that we discuss in Sec. III, which permits a factorization of the microscopic problem into a set of tractable single-bond calculations. Furthermore, we show how to use these microscopic rules in order to construct the complete distribution of transit times for tracer to traverse the system under investigation. This gives rise to a calculated approach which yields, in principle, *exact* values for moments of the transit-time distribution for tracer to pass through a given configuration of

the network. In some respects, the present approach is complementary to the previously developed "probability propagation" algorithm for describing tracer motion on random networks.[11,12]

The aforementioned microscopic rules for the tracer motion are essentially those of a continuum random walker moving in the presence of an inhomogeneous bias whose magnitude is determined by the local flow velocity. This represents the appropriate generalization of random walks in disordered media to account for a finite macroscopic flow in a physically meaningful way. Thus we believe that our general formalism provides an important step in the realistic understanding of flow through porous media.

With our calculational method, we have first studied analytically a number of simple illustrative examples from which we can develop an intuition for the form of the transit-time distribution in the interesting case of a random medium with percolation disorder. We have then implemented our approach numerically for percolating networks at the percolation threshold on $L \times L$ square lattices. Our results suggest that at zero flow velocity, the transit-time moments are all characterized by a single time scale, i.e., $\langle t^k \rangle \sim \langle t \rangle^k$, where $\langle t^k \rangle$ is the kth moment of the transit time. However, at high flow rates, we find that two characteristic time scales are needed to account for the behavior of the moments. This is somewhat reminiscent of the infinity of time scales needed to account for the transit-time moments on a hierarchical structure in the purely convective limit.[13] We are therefore led to postulate a scaling form for the transit-time distribution which is based on a two-time-scale hypothesis. This scaling ansatz is found to account for our data as a function of the flow rate and the system size with a high degree of accuracy.

From our data, we also investigate the behavior of the longitudinal dispersion coefficient $D_{\parallel}$ as a function of system size and of the flow rate. At low values of the flow rate, $D_{\parallel}$ is velocity independent and is governed by $D_{\rm ant}$, the diffusion coefficient of the "ant in the labyrinth."[14] On the other hand, at high flow rate, $D_{\parallel}$ is found to scale as $U^2L^2/D_{\rm ant}$, where U is the average fluid velocity. This form closely parallels the classical Taylor formula for dispersion in a long pipe,[15,16] and, in particular, agrees with a prediction of de Gennes[17] for dispersion on percolation clusters.

This paper is organized as follows. In Sec. II we present a general discussion of the basic physical mechanisms underlying dispersion in random networks, and then consider dispersion in a homogeneous system on the basis of the solution to the macroscopic convection-diffusion equation. In Sec. III we describe our basic formalism for calculating the transit-time distribution for an arbitrary random network of tubes. In Sec. IV we present a physical argument to account for the behavior of the transit-time moments on a simple network whose behavior appears to typify that found on percolation clusters. In particular, the special features associated with the dead ends are emphasized. We then use the formalism of Sec. III to calculate the transit-time moments analytically for a linear chain with any number of dead ends attached to the midpoint. From these examples, the qualitative nature of the transit-time moments for a percolating network may be inferred. In Sec. V we present our numerical simulations and analysis of dispersion on percolating square-lattice networks. A number of results related to the solution of the network convection-diffusion equations, as well as various calculational details, are given in Appendixes A–D.

II. GENERAL DESCRIPTION OF DISPERSION

The nature of hydrodynamic dispersion in porous media is controlled by the competition between convection and molecular diffusion. This competition is embodied by the Péclet number

$$\mathcal{P}=\frac{Ul}{D_m} , \tag{1}$$

where U is the average fluid velocity, l is a characteristic internal length scale of the medium, and D_m is the molecular diffusion coefficient. One may think of $\mathcal{P}$ as the ratio of the molecular diffusion time l^2/D_m to the convection time l/U over a distance l. For small values of the Péclet number, the transport is dominated by molecular diffusion, so that as $\mathcal{P}\to 0$ the dispersion coefficient $D_{\parallel}$ is simply proportional to D_m. More precisely,

$$\frac{D_{\parallel}}{D_m}=\frac{\sigma}{\phi\sigma_0} \quad \text{as } \mathcal{P}\to 0 , \tag{2}$$

where ϕ is the porosity (more generally the volume fraction of the porous material occupied by the fluid), σ_0 is the electrical conductivity of the pore fluid, and σ is the effective conductivity of the porous medium when occupied by the fluid. While this result seems to be well known, we are unable to cite a proof in the literature, and for completeness one is presented in Appendix A.

As the Péclet number increases, the behavior of the dispersion coefficient depends crucially on the connectedness of the system. For a well-connected pore space, both the transport and the mixing of tracer between various streamlines becomes dominated by convection, and $D_{\parallel}$ becomes linear in the flow rate (apart from logarithmic corrections; see below). A simple argument in the spirit of a mean-field approximation can be developed to account for this behavior of the dispersion coefficient. Consider a well-connected network in which the typical spacing between junctions is l (Fig. 1). At the junctions mixing occurs, in which the fluid velocity is changed, both in direction and in magnitude. As a rough approximation to this situation, we replace the random network by a bundle of noninteracting stream tubes which all meet at perfect mixing chambers interspersed a distance l apart. With respect to the average flow velocity U the tracer in a given stream tube may be moving downstream either faster or slower than U. Thus the dispersion process may be viewed as an effective random walk with a characteristic step length l, and a characteristic time between steps given by $\tau=l/U$. Therefore, with respect to the average flow, the spread of tracer will be governed by a dispersion coefficient that scales simply as $l^2/\tau\sim Ul$, and this leads to

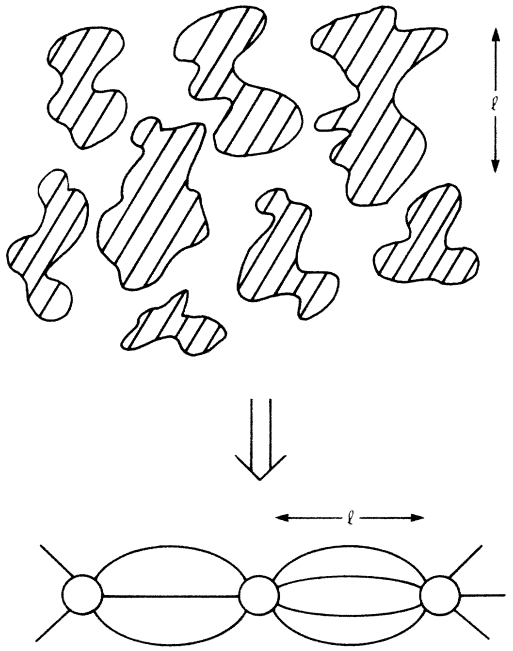

FIG. 1. Schematic picture of a random medium, and its idealization as a bundle of independent stream tubes with mixing occurring only at perfect mixing chambers.

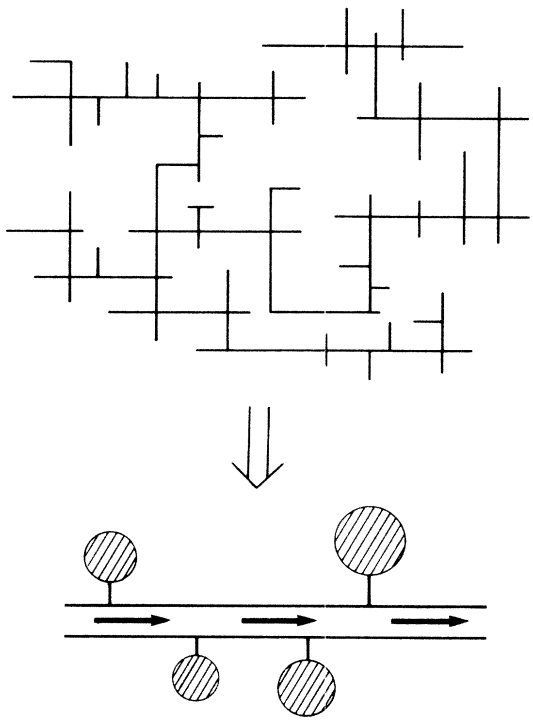

FIG. 2. An idealization of a percolation cluster as a quasi-one-dimensional chain, to which dead ends of length $\mathcal{L}$ are attached.

$$\frac{D_{\parallel}}{D_m} \sim \mathcal{P} . \tag{3}$$

In a more rigorous discussion of this random-walk model, it is necessary to perform an integration over the complete distribution of bond transit times in the porous medium in order to compute typical time scales.[18,19] If the medium contains regions of very slow moving fluid, then one finds that $\langle \tau \rangle$ remains well defined, but that $\langle \tau^2 \rangle$ diverges unless a large-time cutoff is introduced in the bond transit time to render the integral finite. Such a cutoff on the transit time is imposed physically by molecular diffusion, and it ultimately leads to the following logarithmic correction to the dispersion coefficient:[19,20]

$$\frac{D_{\parallel}}{D_m} \sim \mathcal{P} \ln \mathcal{P} . \tag{4}$$

A very different situation occurs when the mixing process is dominated by molecular diffusion, as might occur when there are substantial regions of the pore space where the flow essentially vanishes, or if the tracer can diffuse in and out of the solid grains. Because of such "stagnation" effects, one finds that $D_{\parallel}$ grows quadratically with the flow rate,

$$\frac{D_{\parallel}}{D_m} \sim \mathcal{P}^2 . \tag{5}$$

This behavior can also be understood in simple terms by a random-walk argument. As a rough approximation for distinguishing the flowing and stagnant regions, consider a one-dimensional chain, to which are attached dead ends of a typical length $\mathcal{L}$ (Fig. 2). Tracer is convected through the backbone, while tracer diffuses on the dead ends with diffusion coefficient $D_{\mathcal{L}}$ (which could depend on $\mathcal{L}$ as well as the physical properties of the dead end). Thus with respect to the average flow velocity, the tracer in the dead ends is moving slower than the average, while the tracer in the backbone is moving faster than the average. Once again, the dispersion process may be viewed as an effective random walk with respect to the average flow. The characteristic time τ between successive steps is the typical time for tracer to explore a dead end, and this scales as $\mathcal{L}^2/D_{\mathcal{L}}$. Furthermore, the step length l of the random walk is simply $U\tau$, so that the dispersion coefficient scales as

$$D_{\parallel} \sim l^2/\tau \sim U^2\mathcal{L}^2/D_{\mathcal{L}} . \tag{6}$$

This form for the dispersion coefficient resembles the result obtained by Taylor[15] and Aris[16] for the enhancement of the molecular diffusivity due to Poiseuille flow in a pipe.[21]

If we now consider a flow taking place in a percolating network near the threshold, we have a situation somewhat analogous to flow in a pipe, as the connectivity of the random network is rather tenuous, leading to large (in fact, dominant) dead-end regions. For this case, de Gennes[17] has made the prediction

$$D_{\parallel} \sim \frac{U^2\xi^2}{D_{\text{ant}}} , \tag{7}$$

where ξ is the percolation correlation length and D_{ant} is the microscopic diffusion coefficient of the "ant in the la-

byrinth."[14] This result is of the same form as that given in (6), except for the identification of $\mathcal{L}$ with the correlation length and $D_{\mathcal{L}}$ by $D_{\rm ant}$, both intuitively plausible assumptions. One of the goals of this paper is to investigate the validity of Eq. (7).

Having developed an intuition for the microscopic basis of dispersion, we now turn to a macroscopic description of the process. The conventional approach[1-3] is to view a randomly porous medium as an effective homogeneous system in which the dispersion is described by the convection-diffusion equation (CDE)

$$\frac{\partial C}{\partial t}+U\frac{\partial C}{\partial x}-D_{\parallel}\frac{\partial^2 C}{\partial x^2}-D_{\perp}\nabla_{\perp}^2 C=0\ , \tag{8}$$

where C is the tracer concentration, U is the average flow velocity, assumed to be in the x direction, and $D_{\parallel}$ and $D_{\perp}$ are the longitudinal and transverse dispersion coefficients. The validity of (8) depends essentially on the size L of the system being large enough for the central limit theorem to apply. If we consider a system which is homogeneous only above a scale l, then we clearly require

$$\frac{L}{l}\gg 1\ . \tag{9}$$

However, we also require that the transit time across the entire sample be much greater than any "microscopic" time τ in the system, i.e.,

$$\frac{L}{U}\gg\tau\ , \tag{10}$$

so that the tracer is likely to fully sample the microscopic structure. If the system is purely convective, then τ will be just l/U, and (10) will reduce to (9). However, if there are dead-end regions (for example, of linear extent $\mathcal{L}$) then (10) must also be satisfied for diffusive times τ of order $\mathcal{L}^2/D_{\mathcal{L}}$, where $D_{\mathcal{L}}$ is an effective diffusion coefficient on the scale $\mathcal{L}$. Thus we require

$$\frac{L}{\mathcal{L}}\gg\frac{U\mathcal{L}}{D_{\mathcal{L}}} \tag{11}$$

for an effective macroscopic description to apply.

In order to interpret the results of our numerical simulations, we require the solution of the CDE (8) with boundary conditions appropriate for a macroscopically one-dimensional flow on a finite-length system. The transverse variation will play no role in the subsequent discussion. We consider an initially empty system, and boundary conditions of a unit source of flux at the inlet end and an absorbing boundary at the outlet end of the system. For a system of length L, this leads to

$$\begin{aligned} &C(x,\,t=0)=0\ ,\\ &J(x=0,\,t)=\delta(t)\ ,\\ &C(x=L,\,t)=0\ , \end{aligned} \tag{12}$$

where $J\equiv UC-D_{\parallel}\partial C/\partial x$ is the flux. (Note the two contributions to the flux arising from convection and dispersion, respectively.) The one-dimensional CDE is most conveniently solved by introducing the Laplace transform

$$\tilde{C}(x,s)=\int_0^{\infty}C(x,t)e^{-st}dt\ , \tag{13}$$

which yields for (8)

$$s\tilde{C}(x,s)+U\frac{\partial\tilde{C}(x,s)}{\partial x}-D_{\parallel}\frac{\partial^2\tilde{C}}{\partial x^2}=0\ . \tag{14}$$

The solution to (14) is of the form

$$\tilde{C}(x,s)=Ae^{\alpha x}+Be^{\beta x}\ , \tag{15}$$

where $\alpha,\beta=[U\pm(U^2+4D_{\parallel}s)^{1/2}]/(2D_{\parallel})$ and the constants A and B are determined from the boundary conditions to be

$$\begin{aligned} A&=[D_{\parallel}(\beta-\alpha e^{(\alpha-\beta)L})]^{-1}\ ,\\ B&=[D_{\parallel}(\alpha-\beta e^{-(\alpha-\beta)L})]^{-1}\ . \end{aligned} \tag{16}$$

Finally, we observe that the first-passage probability density $P(t)$ is just the flux at the outlet, a correspondence which arises from the imposed initial conditions of a unit flux input and the presence of an absorbing boundary at the outlet. Thus the Laplace transform of $P(t)$ is

$$\tilde{P}(s)=\tilde{J}(L,s)=\frac{M_s e^{M}}{M\sinh M_s+M_s\cosh M_s}\ , \tag{17}$$

where

$$M=\frac{UL}{2D_{\parallel}} \tag{18}$$

is the *macroscopic* Péclet number, and where

$$M_s=(M^2+sL^2/D_{\parallel})^{1/2}\ . \tag{19}$$

From the definition of Laplace transform, $\tilde{P}(s)$ can be regarded as the generating function of the transit-time moments, which can be extracted by a series expansion of $\tilde{P}(s)$ in powers of s. We thereby obtain

$$\langle t\rangle=\frac{L^2}{D_{\parallel}}\left[\frac{1}{2M}-\frac{1}{4M^2}(1-e^{-2M})\right]\ , \tag{20}$$

$$\langle t^2\rangle=\left[\frac{L^2}{D_{\parallel}}\right]^2\left[\frac{1}{4M^2}-\frac{1}{8M^4}[2-(6M+1)e^{-2M}-e^{-4M}]\right]\ , \tag{21}$$

and so on. The limiting forms of the moments are instructive: For the first moment, we find

$$\langle t\rangle\to\begin{cases}\dfrac{L^2}{2D_{\parallel}} & \text{as } M\to 0 \qquad (22)\\[2ex] \dfrac{L}{U}-\dfrac{D_{\parallel}}{U^2} & \text{as } M\to\infty\ , \qquad (23)\end{cases}$$

while for the second moment, the asymptotic forms are

$$\langle t^2\rangle \to \begin{cases} \frac{5}{12}\left[\frac{L^2}{D_\parallel}\right]^2 & \text{as } M\to 0 \quad (24) \\ \frac{L^2}{U^2}-\frac{2D_\parallel^2}{U^4}+O(e^{-M}) & \text{as } M\to\infty, \quad (25) \end{cases}$$

and the limiting behavior for an arbitrary moment has the form

$$\langle t^k\rangle \to \begin{cases} x_k\left[\frac{L^2}{D_\parallel}\right]^k & \text{as } M\to 0 \quad (26) \\ \left[\frac{L}{U}\right]^k+\cdots & \text{as } M\to\infty, \quad (27) \end{cases}$$

where the x_k are constants. These results are in accord with simple intuition: At small Péclet numbers, the transit-time moments are all governed by the diffusion time $L^2/D_\parallel$, while at high Péclet numbers the moments are governed by the convection time L/U, with correction terms being both of power-law and exponential order in M. For future use, we record the relation between $D_\parallel$ and the transit-time variance $\sigma_t^2\equiv\langle t^2\rangle-\langle t\rangle^2$ in the two limits of small and large Péclet number:

$$D_\parallel \to \begin{cases} \frac{L^2}{\sqrt{6\sigma_t^2}} & \text{as } M\to 0 \quad (28) \\ \frac{U^3}{2L}\sigma_t^2 & \text{as } M\to\infty. \quad (29) \end{cases}$$

In principle, formulas (28) and (29) apply only if the macroscopic CDE provides a good description of the behavior of the system on the length scale L. Necessary conditions for this to be true were given above in (9), (10), and (11). However, the high Péclet-number result (29) can hold under the more general assumption that the system size L is sufficiently large that if we consider a still larger system made up of subsystems of size L, then the different subsystems are "independent," in the sense that tracer will not diffuse against the flow on a length scale L. This requires that the convection time L/U across a length L be much less than the diffusion time L^2/D_L, i.e.,

$$\frac{UL}{D_L}\gg 1 . \quad (30)$$

If this is true, the average time $\langle t\rangle$ for a system of length NL will be just N times that for a system of length L, and similarly for the variance σ_t^2,

$$\sigma_t^2(NL)=N\sigma_t^2(L) . \quad (31)$$

From this, we see that if N is large enough for (29) to hold for a system of size NL, then the correct macroscopic value of $D_\parallel$ will be obtained from

$$D_\parallel=\frac{U^3}{2NL}\sigma_t^2(NL)=\frac{U^3}{2L}\sigma_t^2(L) , \quad (32)$$

i.e., $D_\parallel$ may be obtained by simulations or experiments on a sample of size L, despite the fact that the macroscopic CDE may not be a valid description of the system on that scale. For example, we see that at fixed system size L, the condition (30), required for (31) to be valid, is always satisfied as $U\to\infty$, whereas condition (11), required for the validity of the CDE, is always violated.

Even in cases where the CDE is not strictly applicable, one can obtain useful order-of-magnitude information from equations such as (28) and (29). Consider, for example, diffusion on a percolation cluster, where a simple one-equation macroscopic equation may not be expected to apply. One might, however, make the weaker assumption that the scaling behavior is entirely controlled by D_{ant}, in which case dimensional analysis implies that $\langle t^k\rangle\sim[L^2/D_{\text{ant}}(L)]^k$. The CDE gives this same dependence, but with a specific value of the L-independent prefactor. As we shall show in Sec. V C, the variation with L is indeed as stated, but the prefactor predicted by the CDE is incorrect. More generally, when one examines the transport coefficients of systems as a function of size, there is a strong systematic size variation up to the correlation length, beyond which there is a residual order-of-1 variation until the macroscopic value sets in. We anticipate that one may match a microscopic calculation at the correlation length to the macroscopic equation, to obtain at least the rough size variation of the macroscopic coefficients, if not their precise value.

A common practical remedy for the failure of the CDE, for example, in dispersion in flow in hydrocarbon reservoirs,[22] is to divide the tracer into "flowing" and "stagnant" components. The flowing component is assumed to satisfy the CDE with a capacitancelike coupling to the stagnant tracer. This method is intended to treat situations where the sample is somewhat too short for proper sampling of the pore space to occur, cf. Eq. (11), rather than percolation disorder, and we do not pursue it further here.

III. NETWORK EQUATIONS

The one-dimensional CDE, presented in Sec. II, provides the exact solution of dispersion for a homogeneous one-dimensional system (or equivalently for a single tube) when transverse degrees of freedom are neglected. We shall now extend this calculational approach to treat a random network of such tubes. We describe the tracer concentration in each tube by a one-dimensional CDE involving the molecular diffusivity, thereby assuming that there is perfect transverse mixing. This would be exact in the limit of vanishing tube radius. (To account for a finite tube radius, we may still employ the one-dimensional CDE, but now with the Taylor dispersivity instead of the molecular diffusivity; the formalism of this section would then be unchanged.) We will also assume that there is complete mixing of the tracer at the nodes of the network, so that each tube "sees" the rest of the system only through the tracer concentration at its two ends. By the description of each tube in terms of a CDE, the competition between convection and molecular diffusion is treated in a physically meaningful way according to the degree of local bias in each bond. Owing to the continuum nature of our approach, the effects of

longitudinal dispersion in the links are treated exactly, but the method does rely on the perfect mixing assumptions just stated, so that it becomes exact only in the limit of very narrow tubes.

For well-connected media, the model is perhaps not completely realistic (especially at high Péclet numbers), because regions of slowly moving fluid near the pore walls, and the lack of complete mixing at the nodes are important effects—real porous media do not entirely resemble a network of narrow tubes. However, for poorly connected media, a tube network with percolation disorder offers a reasonable description of a random medium because the dominant transport mechanisms are convection and diffusion over distance scales of order the correlation length, which is much larger than the length of a single tube. Furthermore, at a percolation threshold, one may anticipate that the results will be universal with respect to the details of the microscopic geometry.

In our numerical simulation method, we consider a lattice network of nodes i connected by links ij of length l_{ij} and cross-sectional area S_{ij}. For simplicity, these quantities will be taken to be identical for each link, but the method could easily be extended to the more general case. The nodes at one end of the network are all connected to an inlet node I, and those at the other end to an outlet node O; see Fig. 3. We first compute the background flow field by applying a fixed pressure drop between the inlet and outlet nodes. If there is Poiseuille flow in the tubes, then the fluid flow problem is isomorphic to current flow in a random resistor network for which the conductance of the link ij is given by

$$g_{ij} \sim \frac{S_{ij}^2}{l_{ij}} . \tag{33}$$

The analogy with the resistor network also implies the correspondences

node voltages↔node pressures ,

link currents↔link fluxes .

By a simple rescaling of the pressures at each node, the average flow velocity U may be set to any desired value. In each link there will then be a corresponding value of the local velocity, and the tracer motion in the links is taken to be governed by a one-dimensional CDE, with the drift term given by this local velocity.

This description of the tracer motion should be contrasted with that of a *discrete* (in time and space) biased random-walk model on a percolating cluster.[23–25] One important point of departure is that in typical biased random-walk descriptions, the mean free path coincides with the tube length. By contrast, our formulation of a single tube in terms of a CDE means that we are also considering a biased random walk in each tube, but one in which the ratio of the mean free path to the tube length vanishes. This should be more appropriate for describing tracer motion in a fluid, where the mean free path is negligible compared to the scale of the pores. In the discrete model, the asymptotic behavior of a single tube can be recovered with some calculational labor by a generating-function solution, discussed in great detail by Goldhirsch, Gefen, and co-workers.[24]

A second point of contrast with discrete random-walk models is that in our description there is simple unbiased diffusion (in the continuum limit) in the dead ends, while biased diffusion occurs on the backbone, with the bias in each tube determined by the solution of the global flow equations. However, in biased random-walk models, it is typically assumed that there is a uniform bias everywhere, *including* the dead ends.[26] This leads to dead-end residence times which grow exponentially with the length l of the dead end, rather than growing as l^2 for unbiased diffusion. Consequently, trapping in the dead ends plays a crucial role in determining the motion of a random walker. This might be appropriate for an extremely dilute system where hydrodynamics is not relevant, but not for typical fluids.

As in the single-tube problem, the fundamental quantity describing transport in the network is the first passage probability density $P(t)$ for the tracer to arrive at the outlet node, given that there is a δ-function injection of flux at the inlet node. This first-passage problem may be solved in terms of the set of local tracer concentrations, $\{c_i(t)\}$, at the nodes of the network. To solve for the $\{c_i(t)\}$, first consider the equation of motion for a single link ij in which the tracer concentration within the link, $c_{ij}(x,t)$, satisfies

$$\frac{\partial c}{\partial t} + u\frac{\partial c}{\partial x} - D_m \frac{\partial^2 c}{\partial x^2} = 0 , \tag{34}$$

where $u = u_{ij}$ is the local flow velocity in the link (with the sign convention that flow from i to j is considered positive) and $c = c_{ij}$. If, initially, $c_{ij}(x, t=0) = 0$ for all links, then in the Laplace transform domain Eq. (34) becomes

$$s\tilde{c} + u\frac{\partial \tilde{c}}{\partial x} - D_m \frac{\partial^2 \tilde{c}}{\partial x^2} = 0 . \tag{35}$$

The boundary conditions appropriate for the system are determined by the continuity of the various link tracer concentrations at a junction between several links. That is,

$$\begin{aligned} \tilde{c}_{ij} &= \tilde{c}_i \quad \text{at } x = 0 , \\ \tilde{c}_{ij} &= \tilde{c}_j \quad \text{at } x = l_{ij} . \end{aligned} \tag{36}$$

As in Sec. II, the solution to (35) is of the form

$$\tilde{c}(x,s) = Ae^{\alpha x} + Be^{\beta x} , \tag{37}$$

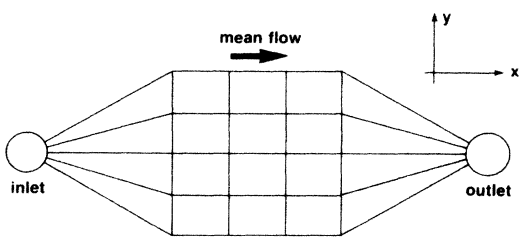

FIG. 3. Typical network configuration used for computer simulations.

where

$$\alpha,\beta=\frac{u\pm(u^2+4D_m s)^{1/2}}{2D_m} , \tag{38}$$

and for the boundary conditions specified,

$$A=\frac{\tilde{c}_j-\tilde{c}_i e^{\beta l}}{e^{\alpha l}-e^{\beta l}} ,$$
$$B=\frac{\tilde{c}_i e^{\alpha l}-\tilde{c}_j}{e^{\alpha l}-e^{\beta l}} . \tag{39}$$

The Laplace transform of the flux leaving node i along link ij is then given by

$$\tilde{J}_{ij}=S_{ij}\left[u_{ij}\tilde{c}_{ij}-D_m\frac{\partial\tilde{c}_{ij}}{\partial x}\right]_{x=0} . \tag{40}$$

Using Eqs. (37)–(39), we may express this flux in terms of the concentrations $\tilde{c}_i$ and $\tilde{c}_j$ at the two ends. Thus writing $\tilde{J}_{ij}=G_{ij}^{+}\tilde{c}_i-G_{ij}^{-}\tilde{c}_j$, we find

$$G_{ij}^{+}(s)=D_m S_{ij}(m+m_s\coth m_s)/l , \tag{41}$$

$$G_{ij}^{-}(s)=D_m S_{ij}(m_s e^{-m}/\sinh m_s)/l , \tag{42}$$

where $m=ul/2D_m$ and $m_s=(m^2+sl^2/D_m)^{1/2}$. Assuming that the nodes have negligible volume, then the tracer cannot accumulate at these points, so that the $\tilde{c}_i$ satisfy

$$0=\sum_j \tilde{J}_{ij}=\sum_j (G_{ij}^{+}\tilde{c}_i-G_{ij}^{-}\tilde{c}_j) \tag{43}$$

for the interior nodes, and

$$1=\sum_j \tilde{J}_{Ij}$$
$$=\sum_j (G_{Ij}^{+}\tilde{c}_I-G_{Ij}^{-}\tilde{c}_j) \tag{44}$$

for the inlet node (corresponding to a δ-function input of flux). Due to the absorbing boundary condition at the outlet node, the Laplace transform of the first-passage probability density $P(t)$ is simply given by the flux exiting via the outlet node

$$\tilde{P}(s)=-\sum_j \tilde{J}_{Oj}=\sum_j G_{Oj}^{-}\tilde{c}_j . \tag{45}$$

For any given value of s the Eqs. (43) and (44) and the associated boundary conditions are the analogues of the Kirchhoff equations $\sum_j g_{ij}(v_i-v_j)=0$, for the potentials v_i in an electrical network. The primary difference between the two sets of network equations is that in the tracer problem, the effective link conductances are direction dependent. In other words, when the network equations are written in the matrix form

$$\underline{A}(s)\underline{\tilde{c}}(s)=\underline{b} , \tag{46}$$

then the matrix $\underline{A}(s)$ is not symmetric. Note that, because we consider a δ-function input of flux, the right-hand side, $\underline{b}$, of (46) is independent of s.

The simultaneous equations (46) may be solved in a number of ways.[11,27,28] In Ref. 11, they were solved by a "probability propagation" algorithm which was motivated by a physical picture in which individual packets of first-passage probability representing summations over all possible paths of tracer particles are propagated through the system. In fact, it is possible to show that the network first-passage probability (45) is obtained exactly, up to geometric convergence, from the probability propagation algorithm. (This relation is elucidated in Appendix B.) For a well-connected network with little backflow or stagnation effects, probability propagation leads to a relatively efficient method as the computation time is proportional to the system volume. It should also be emphasized that probability propagation represents an exact summation over all possible tracer particle paths through the network. Consequently, probability propagation should supersede earlier computational approaches, based on the passage of individual particles through the network.[4,5] In fact, the latter approach *must* lead to incorrect results in a finite simulation, as the low-probability paths, which can dominate the higher transit-time moments, will not be sufficiently well sampled. (To be fair, the work of Sahimi *et al.*[4,5] concerns the *purely* convective limit where probability propagation is quite equivalent to particle tracking; further discussion of this question is given by Sahimi and Imdakm.[29])

For a poorly connected medium, on the other hand, backflow and stagnation cause the propagation of first-passage probability to become relatively inefficient. As an alternative, Roux *et al.*[27] solved the network equations by a transform matrix method, in close analogy with a similer method used for electrical networks. Here, as in Ref. 28, we will simply solve the equations, directly, using a standard inversion routine for nonsymmetric matrices. There are two variations of this approach which we have used to obtain complementary information. First, we may simply solve Eq. (46) at selected values of the Laplace transform variable s, compute $\tilde{P}(s)$ from (45), and then use a numerical inversion to convert to the time domain and finally obtain $P(t)$. However, if we are interested only in the transit-time moments

$$M_n=\int_0^\infty dt\, P(t)t^n , \tag{47}$$

then we may expand $\underline{A}(s)$ and $\underline{\tilde{c}}(s)$ in powers of s,

$$\underline{A}(s)=\underline{A}^{(0)}+\underline{A}^{(1)}s+\underline{A}^{(2)}s^2+\cdots , \tag{48}$$

$$\underline{\tilde{c}}(s)=\underline{\tilde{c}}^{(0)}+\underline{\tilde{c}}^{(1)}s+\underline{\tilde{c}}^{(2)}s^2+\cdots , \tag{49}$$

so that by equating powers of s in (46) we obtain

$$\underline{A}^{(0)}\underline{\tilde{c}}^{(0)}=\underline{b} ,$$
$$\underline{A}^{(0)}\underline{\tilde{c}}^{(1)}=-\underline{A}^{(1)}\underline{\tilde{c}}^{(0)} , \tag{50}$$
$$\underline{A}^{(0)}\underline{\tilde{c}}^{(2)}=-\underline{A}^{(1)}\tilde{c}^{(1)}-\underline{A}^{(2)}\underline{\tilde{c}}^{(0)} ,$$

etc. The moments are then given by

$$M_n=(-1)^n n!\sum_j\sum_{m=0}^{n} G_{Oj}^{-(m)}\tilde{c}_j^{(n-m)} , \tag{51}$$

where $\sum_j$ denotes a sum over the nodes connected to the outlet, and the $G_{Oj}^{-(m)}$ are obtained by expanding $G_{Oj}^{-}(s)$ in powers of s,

$$G_{\bar{O}j}(s)=G_{\bar{O}j}^{(0)}+G_{\bar{O}j}^{(1)}s+G_{\bar{O}j}^{(2)}s^2+\cdots . \quad (52)$$

We see that in order to obtain the moments, it is only necessary to invert the matrix $\mathbf{A}^{(0)}$.

IV. HIGH-PÉCLET-NUMBER LIMIT FOR SMALL NETWORKS

Many of the results we shall obtain for the transport of tracer on percolating networks in the limit of Péclet number can be anticipated on the basis of analytical results for a small network containing a dead end. This particular example appears to capture the essential nature of the competition between convection and diffusion in the high-Péclet-number limit. Additionally, this example suggests the general behavior for the transit-time moments which, in fact, accounts for our numerical data on percolation networks. We shall begin with our heuristic argument for the form of the moments, and then verify that these moments are qualitatively correct by using the detailed microscopic rules of Sec. III.

Consider the Y-shaped network shown in Fig. 4, where the incoming fluid flux q branches into two tubes of respective fluxes ϵq and $(1-\epsilon)q$. It is pedagogically useful to think of the "weaker" branch as approaching a dead end as the limit $\epsilon\to 0$ is taken. In this system, the tracer flux through each branch may be viewed as the sum of diffusive and convective processes which occur independently and simultaneously. The total transition rate into the upper tube is then the sum of its diffusive rate, equal to the inverse diffusion time D_m/l^2, and its convective rate, equal to the inverse convection time $u/l=\epsilon q/v$, where u is the upper branch velocity and v is the tube volume. A similar expression applies to the lower branch, and each transition rate is the relative probability of tracer traversing the respective tube. As $\epsilon\to 0$, these rates tend to D_m/l^2 and q/v for the upper and lower branches, respectively, and the relative entrance probabilities tend to $p_u=D_m v/l^2 q+O(q^{-2})$ and $p_l=1-p_u$. (These results for the respective probabilities can be obtained rigorously using the probability-propagation ideas of Ref. 11.) Thus the moments of the transit-time distribution are, to leading order in q^{-1},

$$\langle t^k\rangle = p_u t_u^k + p_l t_l^k \sim \frac{D_m v}{l^2 q}\left[\frac{v}{q}+\frac{l^2}{D_m}+\frac{v}{q}\right]^k + \left[\frac{v}{q}+\frac{v}{q}\right]^k . \quad (53)$$

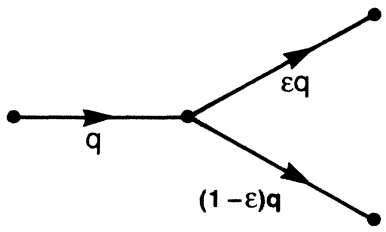

FIG. 4. Simple network illustrating the approach to the diffusive limit.

We can rewrite this result in the more general (and suggestive) form

$$\langle t^k\rangle \sim \tau_C \tau_D^{k-1} , \quad (54)$$

where $\tau_C=\langle t\rangle=3v/q$ is the "convection time," which in turn is equal to the total volume of the system divided by the flux, and $\tau_D=l^2/D_m$ is the "diffusive time" in the dead end. Thus the contribution of the slowest bond dominates in all but the first moment, in which case this contribution is of the same order as that of the rest of the network.

We now verify the heuristic reasoning just given, by using the formalism of Sec. III (similar results were first obtained by Aris[30] using a different method based on moments of the CDE). Let us proceed directly to the Y network in the dead-end limit, which is redrawn for clarity in Fig. 5. The two series bonds have length l, and a dead-end bond is attached to the central node. Suppose that all the bonds have cross-sectional area S, and that the flow velocity on the two "backbone" bonds is u. For generality, suppose the dead-end bond has a different length $\mathcal{L}$, volume V, and diffusivity D than the backbone bonds. We are interested in the transit-time moments of this system in the high-velocity limit. For this purpose, we require the limiting forms of the matrix coefficients G^+ and G^-. Using Eqs. (41) and (42), we see that for the backbone bonds

$$G^+(m,s)\to q , \quad (55)$$

$$G^-(m,s)\to 0 , \quad (56)$$

for $m=ul/2D_m\to+\infty$ (outgoing links), and

$$G^+(m,s)\to 0 , \quad (57)$$

$$G^-(m,s)\to qe^{-sv/q} , \quad (58)$$

for $m\to-\infty$ (incoming lines), where $q=uS$ is the flux in the link and $v=lS$ is the volume of the link. For the dead-end bonds, the limiting forms are

$$G^+(m,s)=\frac{SD}{\mathcal{L}}m_s\coth m_s\sim g+\frac{Vs}{3}+\frac{V\mathcal{L}^2s^2}{45D} \quad \text{as } s\to 0 , \quad (59)$$

$$G^-(m,s)=\frac{SD}{\mathcal{L}}\frac{m_s}{\sinh m_s}\sim g-\frac{Vs}{6}+\frac{7V\mathcal{L}^2s^2}{360D} \quad \text{as } s\to 0 , \quad (60)$$

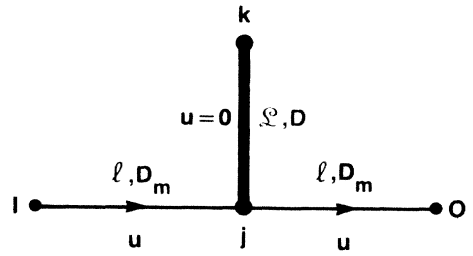

FIG. 5. Geometry of a simple dead-end configuration; bond velocities, lengths and diffusivities are shown.

where $g=SD/\mathcal{L}$ and $V=S\mathcal{L}$.

From the following network equations for each node of the system: inlet node,

$$q\tilde{c}_I=1 \; ; \tag{61a}$$

outlet node,

$$qe^{-sv/q}\tilde{c}_j=\tilde{P}(s) \; ; \tag{61b}$$

dead-end node k,

$$G^+(0,s)\tilde{c}_k-G^-(0,s)\tilde{c}_j=0 \; ; \tag{61c}$$

central node j,

$$qe^{-sv/q}\tilde{c}_I+q\tilde{c}_j+G^+(0,s)\tilde{c}_j-G^-(0,s)\tilde{c}_k=0 \; ; \tag{61d}$$

we may straightforwardly solve for $\tilde{P}(s)$ and obtain

$$\tilde{P}(s)=\frac{qe^{-2vs/q}}{q+S\sqrt{sD}\,\tanh\sqrt{s\mathcal{L}^2/D}} \; . \tag{62}$$

At this stage, the moments of $P(t)$ could be extracted by differentiating (62) directly, but it is slightly more convenient to calculate the *cumulants* by differentiating $\ln\tilde{P}(s)$. Using the fact that, as $q\to\infty$,

$$\ln\tilde{P}(s)\sim-\frac{1}{q}(2vs+S\sqrt{sD}\,\tanh\sqrt{s\mathcal{L}^2/D}) \; , \tag{63}$$

we obtain

$$\langle t\rangle=\frac{2v+V}{q}=\frac{2l}{U} \; , \tag{64}$$

where $U=2lu/(2l+\mathcal{L})$ is the average velocity in the system. Similarly, for the second cumulant we find

$$\sigma^2\equiv\langle t^2\rangle-\langle t\rangle^2=\frac{\mathcal{L}^3}{3uD} \; . \tag{65}$$

More generally, for $k>1$, the kth cumulant scales as

$$C_k\sim\frac{S\mathcal{L}^{2k-1}}{qD^{k-1}}=f_v\tau_C\tau_D^{k-1} \; . \tag{66}$$

Here $f_v=V/(2v+v)$ is the volume fraction of dead end, $\tau_C=\langle t\rangle$ is the convective transit time across the system, and $\tau_D=L^2/D$ is the diffusive transit time on the dead end. Note also that, to leading order in $1/q$, $C_k\sim\langle t^k\rangle$, and that $C_k/C_{k-1}\sim\mathcal{L}^2/D$, independent of k. The above result for the cumulants agrees with our heuristic arguments above, and we shall see that it also appears to account for our numerical data on percolating networks.

The strikingly simple result given in Eq. (64), that $\langle t\rangle$ equals the pore space volume divided by the flux in the high-Péclet-number limit, is actually quite general. It is proved for an arbitrary network configuration at high Péclet number in Appendix C. A statement equivalent to (64) is that the average transit time equals the system length divided by the average fluid velocity in the pore space or, loosely, that the average tracer velocity equals the average fluid velocity. Since the local velocity of the tracer consists of a fluctuating Brownian term plus a drift given by the local flow field, the latter statement is intuitively reasonable. From the macroscopic point of view, the fact that the mean time equals the pore volume over the flux is equivalent to Eq. (23), and is a consequence of the CDE when the latter applies and when the Péclet number is large, a fact long known in the chemical engineering literature.[31]

The physical implications of this result for the first moment are far reaching as *all* pore space makes an equal contribution to the average transit time, *independent* of the local velocity. This stems from a cancellation of the competing effects of the probability of entering a given region of the system (which is proportional to the local Péclet number), and the expected transit time through this region (which is proportional to the inverse of the Péclet number), in obtaining the average of the transit time.

If we describe the system by a macroscopic CDE, we can now use Eqs. (66) and (29) to write the dispersion coefficient as

$$D_{\parallel}=\frac{U^3}{2(2l)}\sigma^2=f_v\frac{U^2\mathcal{L}^2}{D} \; , \tag{67}$$

where the *average velocity* is $U=2lu/(2l+\mathcal{L})$. This expression is quite similar to de Gennes's prediction (7), but multiplied (very plausibly) by the relative volume of dead end present.

We can bring this simple model into even closer analogy to a percolation network by attaching an arbitrary number of dead ends to the central node j, with each dead end having a length $\mathcal{L}_\alpha$, volume V_α, and a (possibly distinct) microscopic diffusion coefficient D_α. Each dead-end node concentration can be eliminated by the analog of Eqs. (61), and thus makes an independent additive contribution to (63). Thus, at large q,

$$\ln\tilde{P}(s)\sim-\frac{1}{q}\left[2vs+S\sum_\alpha\sqrt{sD_\alpha}\,\tanh\sqrt{s\mathcal{L}_\alpha^2/D_\alpha}\right] \; , \tag{68}$$

from which we find that

$$\langle t\rangle=\frac{2v+\sum_\alpha V_\alpha}{q} \; , \tag{69}$$

and that the cumulants scale as

$$C_k\sim\frac{1}{u}\sum_\alpha\frac{\mathcal{L}_\alpha^{2k-1}}{D_\alpha^{k-1}} \quad \text{for } k>1 \; . \tag{70}$$

The latter expression suggests that the largest dead end in the system dominates the behavior of the cumulants. To see this concretely, suppose that the probability distribution of dead-end lengths is

$$\rho(\mathcal{L})\sim\mathcal{L}^{-x}e^{-\mathcal{L}/\xi} \; , \tag{71}$$

where $\xi\gg l$ is the correlation length, and that the diffusion coefficient on a dead end of length $\mathcal{L}$ varies as $D(\mathcal{L})\sim\mathcal{L}^{-\theta}$, where θ is the ant exponent. Replacing $\sum_\alpha$ by $\int d\mathcal{L}$, we obtain

$$C_k\sim\frac{1}{u}\xi^{2k-x-(k-1)\theta} \; . \tag{72}$$

For $\xi\gg l$ we have

$$U=\frac{2lu}{\sum_{\alpha}\mathcal{L}_{\alpha}}\sim\frac{ul}{\xi^{2-x}}\ , \tag{73}$$

and therefore

$$C_k\sim\frac{l}{U}\xi^{(2+\theta)(k-1)}\sim\tau_C\tau_D^{k-1}\ . \tag{74}$$

We again obtain the same scaling law for the moments as in Eq. (54), where now the diffusion time is controlled by the anomalous diffusion exponent

$$\tau_D\sim\xi^{2+\theta}\ . \tag{75}$$

Note again that it is the *average* velocity over the entire pore space, rather than the backbone velocity, which enters the moments and longitudinal dispersivity.

V. NUMERICAL RESULTS FOR PERCOLATING CLUSTERS

For percolating networks, we have used the formalism developed in Sec. III to calculate the Laplace transforms of the tracer concentrations at each site of the network. From these quantities, we can calculate either the transit-time probability density $P(t)$ by numerical inversion, or the transit-time moments as outlined in Eqs. (47)–(51). We again emphasize that the moments obtained in this manner are exact for a given configuration, up to the round-off error inherent in the numerical solution of the network equations. The same methods can also be used for nonpercolative networks, and to illustrate this point we will also discuss the behavior of the moments on fully occupied lattices.

We consider networks of identical links on a square lattice at the percolation threshold, with the linear dimension L of the lattice ranging from 2 to 70. We choose a self-dual lattice (Fig. 3) so that the percolation threshold occurs exactly at bond occupation probability equal to $\frac{1}{2}$.[32] For each configuration, we first find the background flow field by assuming that each occupied link has flow conductance unity and solving an analog random resistor problem with unit pressure drop. We then scale the resulting fluid flux in each bond by a common factor so that the total flux passing through the network has a (dimensionless) value $\hat{Q}$. The dimensionless average velocity in the network is the flux divided by the average number of bonds *across* the sample, $\hat{U}=\hat{Q}/L^{1-\beta/\nu}$. The rescaled flux in each bond can be taken to coincide with the microscopic Péclet number, since the latter is related to the flux by constant factors which are the same for each bond. Furthermore, the unscaled total flux is the electrical conductivity normalized to the pore fluid conductivity σ/σ_0 and the porosity is just the actual number of bonds present divided by the maximum number allowed. The relation between this dimensionless description and physical units is discussed in detail in Appendix D.

We have typically obtained data for nine different values of $\hat{Q}=0,10^{-2},10^{-1},\ldots,10^{5}$. This range of $\hat{Q}$ values spans both the purely diffusive regime and the extreme convective limit where the average transit time varies strictly linearly with $1/\hat{U}$. Each data point was based on averaging results over 2000–6000 realizations of the network for $L\leq 60$ (and rather fewer for $L=70$ due to computer limitations). The typical standard deviation in the mean ranges from a few percent for the first moment to about 25% for the highest. In addition, for $L=2$ and 3, it is feasible to enumerate and solve all $2^{L^2+(L-1)^2}$ configurations of the network and thereby obtain the exact configurational-averaged transit-time moments. The data obtained in this manner do agree quite accurately with those obtained by a random sampling of the configurations, and this serves as a useful check of our Monte Carlo data.

A. The transit-time probability density

To gain some qualitative insight into the time dependence of the transit-time distribution $P(t)$, we have plotted it for various systems of linear dimension $L=10$. These results were obtained by evaluating $P(s)$ at discrete values of s, and using the Stehfest algorithm[33] to numerically invert the Laplace transform. In Fig. 6, we compare a one-dimensional chain of length 10, a fully-occupied 10×10 lattice, and the average over 100 realizations of a 10×10 lattice at the percolation threshold, all with $\hat{Q}=1$. Because of our asymmetric boundary conditions and the finite size of the system, these curves are all skewed with prominent long-time tails. The dot on each curve identifies the location of $\langle t\rangle$. We see that in going from the linear chain (no dead ends), to the fully occupied lattice (small stagnation zones), to the percolating network (large dead ends), the tail becomes more prominent and the separation between the mean and most probable transit time increases. In Fig. 7, we illustrate the velocity variation of $P(t)$ by comparing the results for percolation lattices at flow rates $\hat{Q}=0$, 0.1, and 1.0. In the purely diffusive limit, $P(t)$ is quite broad, but it sharpens as the flow rate increases and tracer is convected through the system. Further increase of $\hat{Q}$ continues to sharpen the peak and move it to lower values of t, but the curve al-

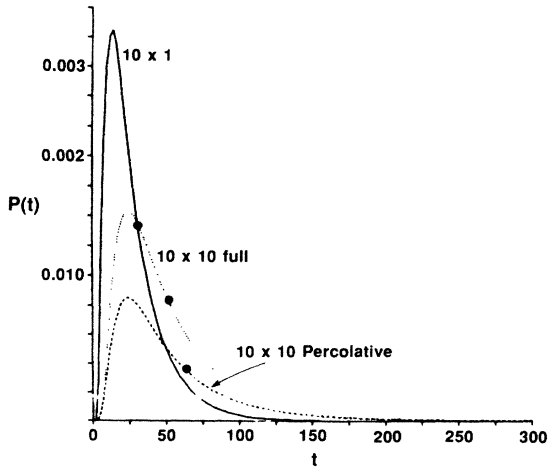

FIG 6. Transit-time probability density for a chain of length 10 (solid line), a 10×10 full lattice (dashed line), and a 10×10 lattice at the percolation threshold (dotted line), all at $\hat{Q}=1.0$.

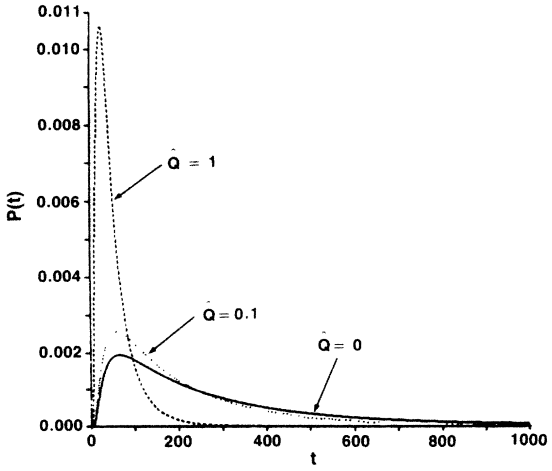

FIG. 7. Transit-time probability density for a 10×10 percolation lattice at $\hat{Q}=0$ (solid line), $\hat{Q}=0.1$ (dashed line), and $\hat{Q}=1.0$ (dotted line).

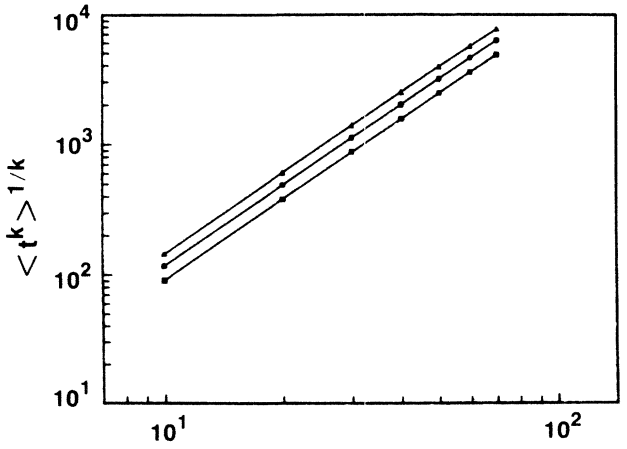

FIG. 8. Variation of $\langle t^k \rangle$ for a fully occupied lattice of size L at $\hat{Q}=0$.

ways remains skewed and always has a long-time diffusive tail.

One conclusion to be drawn from these figures is that the various distributions are similar at a qualitative level, independent of the microscopic structure of the system. There are of course crucial quantitative differences in the curves shown, particularly in the strength of the tail, but they are not readily evident in this presentation. We turn to the transit-time moments, whose qualitative behavior is far more instructive.

B. The fully occupied lattice

As a preliminary to percolation disorder, it is useful to consider the transit-time moments on lattices where all bonds are present. First, in the limit of zero average velocity, there is simple molecular diffusion on a regular lattice of cylindrical tubes. We would therefore expect the diffusion equation to apply and that the effective and molecular diffusivities would coincide. Furthermore, since the macroscopic Péclet number is zero, we expect the simple size-scaling behavior $\langle t^k \rangle \sim L^{2k}$, from Eqs. (22), (24), and (26). In Fig. 8, we plot the first three moments, which indeed behave as indicated, and further the numerical values are in accord with the macroscopic CDE. An additional test of the macroscopic behavior is provided by Eq. (2); in Fig. 9, we compare the diffusivity as given by (28) with the ratio of electrical conductivity to porosity. As the lattice size increases, the two quantities converge to a common value of $\frac{1}{2}$, as anticipated.

We next consider the behavior at high velocities, and we plot the first three moments as a function of $\hat{Q}$ for $L=70$ in Fig. 10, and as a function of size at $\hat{Q}=10^5$ in Fig. 11. (The velocity variation of the transit-time moments for this lattice was first discussed by Roux *et al.*[27]) In the first figure, we see two different regimes of behavior for the moments, which can be interpreted in the following manner. The system considered here consists of horizontal "convective" bonds with high-velocity fluid and volume V_C, say, plus zero-velocity "dead-end" vertical bonds of total volume V_D. In the spirit of the heuristic argument presented in Sec. IV, we would write the moments as

$$\langle t^k \rangle \sim \frac{D_m V_D}{Q l^2} \left[\frac{V_C}{Q} + \frac{l^2}{D_m} \right]^k + \left[\frac{V_C}{Q} \right]^k , \tag{76}$$

where for clarity we employ the quantity Q, which is the flux in physical units (cf. Appendix D). Here the two terms refer to tracer which enters a dead end and must diffuse out, and tracer which simply convects through the network, respectively. Now when the flux is not *too* large, i.e., $V_C/Q \gg l^2/D_m$, one has $\langle t^k \rangle \sim Q^{-k}$ from the second term, whereas in the opposite case of very high flux, the first term dominates to yield $\langle t^k \rangle \sim Q^{-1}$. These two limits correspond to the two regimes in Fig. 10.

Turning next to the size variation of the moments at very high velocity, Fig. 11, we first note that both the heuristic argument just given as well as the average time theorem of Appendix C imply that $\langle t \rangle$ should vary as

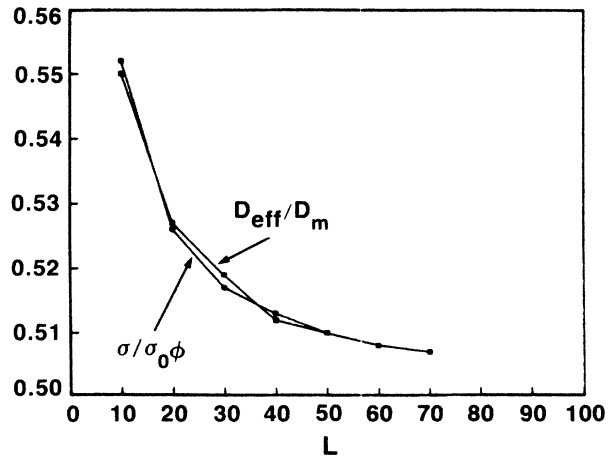

FIG. 9. Comparison of D_{eff} (closed squares) with $\sigma/\sigma_0\phi$ (closed circles) for full lattices at $\hat{Q}=0$.

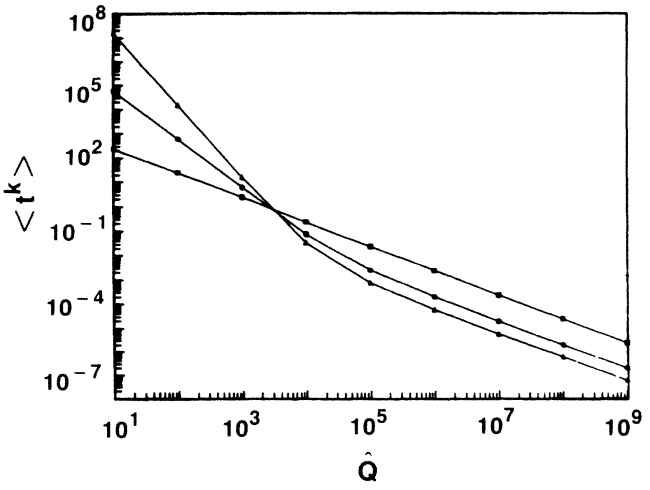

FIG. 10. Variation of $\langle t^k \rangle$ with $\hat{Q}$ for a 70×70 full lattice.

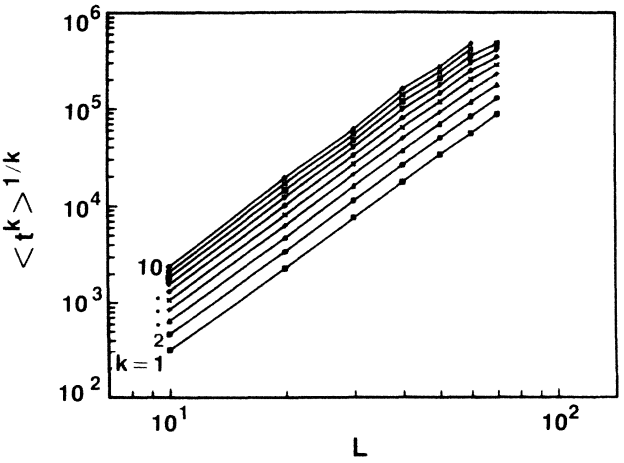

FIG. 12. Variation of reduced moments $\langle t^k \rangle^{1/k}$, $k = 1, 2, \ldots, 10$, for percolation lattices at $\hat{Q} = 0$.

$L^2/\hat{Q}$ once $\hat{Q} \gg 1$. For the other moments, the above argument predicts $\langle t^k \rangle \sim \tau_C \tau_D^{k-1} \sim L^2/\hat{Q}$, because the characteristic diffusion time is simply that of a single bond ($\tau_D \sim l^2/D_m$). The numerical data are in agreement with these estimates.

Lastly, we consider the relevance of the macroscopic CDE for describing the fully occupied lattice; in Sec. III, we argued that a necessary condition for its relevance is Eq. (11), that the tracer spends enough time in the system to sample the pore space fully. We may rewrite this condition in terms of the flux as $V_C/Q \gg l^2/D_m$, which is satisfied only in the intermediate-Q regime. In this case, the arguments of Sec. II suggest that $D_\parallel \sim U^2 l^2/D_m$, and so the macroscopic Péclet number $M = UL/2D_\parallel \sim D_m L/l^2 U \gg 1$. The relevant limiting form of the solution to the CDE is that given in Eq. (27), which has $\langle t^k \rangle \sim Q^{-k}$, in agreement with the numerical data.

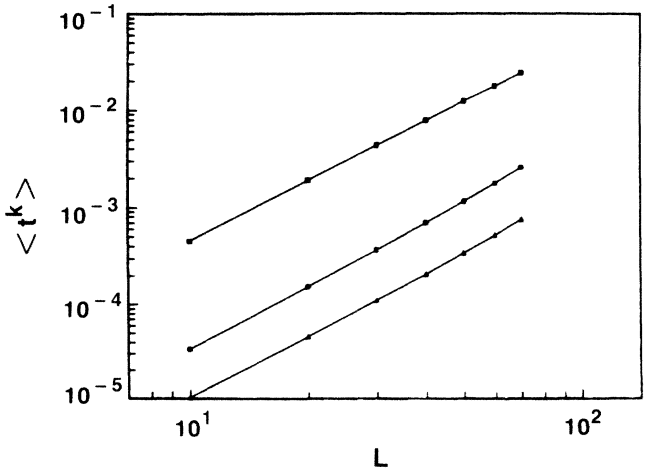

FIG. 11. Variation of $\langle t^k \rangle$ with L for full lattices at $\hat{Q} = 10^5$.

C. Percolation moments at $\hat{Q} = 0$

In the absence of convection, the tracer motion reduces to a continuum version of anomalous diffusion on percolation clusters. As discussed in Sec. II, one expects that the diffusion equation does not apply, but that the transport is controlled by the "ant in the labyrinth" diffusivity. If this is the case, then the scaling law

$$\langle t^k \rangle \sim \left[\frac{L^2}{D_{\text{ant}}(L)} \right]^k \sim L^{k(2+\theta)} \tag{77}$$

is expected, because L^2/D_{ant} is the only time scale in the problem. If the macroscopic diffusion equation were to apply, then one could additionally obtain specific values for the proportionality constants in this equation. In Fig. 12, we plot the reduced moments $\langle t^k \rangle^{1/k}$ versus L for $k = 1, 2, \ldots, 10$. The different curves are indeed parallel, with a common slope 2.9–3.0, as compared to the expected value $2 + \theta \approx 2.86$ in two dimensions. On the other hand, the numerical coefficients do not agree with Eqs. (22) and (24), indicating that a CDE does not apply to these percolation systems. A further verification of the last statement can be made by testing Eq. (2), which is implied by a continuum description. If we use Eq. (28) for the diffusion coefficient, the (numerically computed) actual average number of bonds in the system for the porosity, and the unscaled flux for the conductivity (see Appendix D), we obtain the results given in Fig. 13. The disagreement between the two curves consists approximately of a constant factor independent of L, because the previous results for the moments imply $L^2/(\sigma_t^2)^{1/2} \sim D_{\text{ant}}$, and the L dependence of the latter is usually derived from that of $\phi\sigma$.

D. Percolation moments as $\hat{Q} \to \infty$

The behavior in the high–Péclet-number regime is rather more interesting. First, the reduced moment $\langle t^k \rangle^{1/k}$ now *depends* on k, suggesting that there is no single unique time scale which characterizes the transit-time

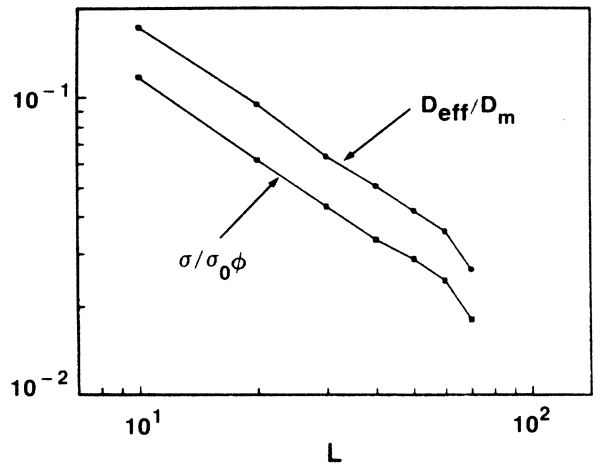

FIG. 13. Comparison of D_{eff} (closed squares) with $\sigma/\sigma_0\phi$ (closed circles) for percolation lattices at $\hat{Q}=0$.

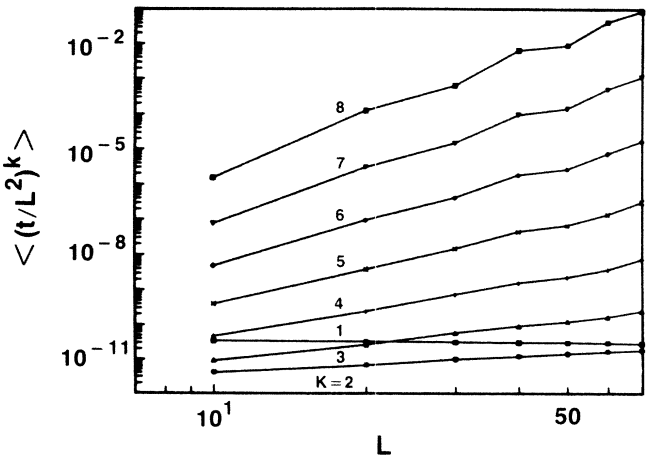

FIG. 14. Variation of $\langle (t/L^2)^k \rangle$ with L for percolation lattices at $\hat{Q}=10^{10}$.

distribution in the high-Péclet-number limit. However, on the basis of the intuition developed in Sec. IV, we expect that $\langle t^k \rangle$ will scale as $\tau_C \tau_D^{k-1}$, where τ_C and τ_D are typical time scales for tracer to convect or diffuse across the network, respectively. For percolating clusters, these two time scales can be inferred on physical grounds. From the theorem that the average transit time at high flow rates is proportional to the volume of the system, we have $\tau_C \sim L^{2-\beta/\nu}/\hat{Q}$, where the L-dependent factor is the average number of bonds in a percolating cluster of an $L \times L$ system. Furthermore, from our numerical results at zero flow rate, there appears to be a unique diffusive time scale $\tau_D \sim L^{2+\theta}$, which governs all the transit-time moments in the diffusive limit.

Combining these two results, we anticipate that

$$\langle t^k \rangle \sim \frac{1}{\hat{Q}} L^{2-\beta/\nu+(k-1)(2+\theta)} . \tag{78}$$

This form appears to provide a reasonable account of the data, as shown in Fig. 14. We show $\langle (t/L^2)^k \rangle$ for $k=1,\ldots,8$ for sizes 10 through 70. The data are fit quite well by a power law for the low moments, but the uncertainties become quite large for $k=7$ or 8, where the standard deviation in the mean is about $\frac{1}{3}$ of the mean itself. The slopes resulting from an approximate straight-line fit are given in Table I, and compared to the expected exponent $-\beta/\nu+(k-1)\theta$. The agreement is quite good, and well within the fluctuations in the numerical data.

As discussed previously, we do not expect the CDE to apply directly to this percolating system, but in accord with our remarks at the end of Sec. II, we can still use the variance σ_t^2 to obtain the macroscopic dispersivity on scales much greater than the correlation length. Thus using $\sigma_t^2 \approx \langle t^2 \rangle$ from our numerical results of this section, $D_{\parallel} \sim U^3 \sigma_t^2 / L$ from (29), and $\hat{U} \sim \hat{Q}/L^{1-\beta/\nu}$ from the definition of average velocity, we thereby find

$$D_{\parallel} \sim \frac{U^2 L^2}{D_{\text{ant}}(L)} , \tag{79}$$

which is in agreement with de Gennes.[17]

Vannimenus[34] has proposed a modified form for $D_{\parallel}$ which is intended to take account of the embedding of fractal structures in Euclidean space. The effect of this modification is to multiply Eq. (7) by a factor $L^{2(d_f/\hat{d}-1)}$, which involves the fractal dimension $d_f=2-\beta/\nu$ and the spectral dimension $\hat{d}$ (respectively, 1.89 and about 1.7 in two dimensions). Unfortunately, our numerical data are not sufficiently precise to check for this weak size dependence ($\sim L^{0.2}$). One might also inquire whether the average velocity used in de Gennes's formula should instead be the *backbone* velocity. If this were the case, β should be replaced by the corresponding backbone exponent, $\beta_{BB} \approx 0.33$ in two dimensions. Again, this leads to a small alteration which varies as $L^{0.14}$ in the predicted moments, and it is difficult to test this variation with our data.

One might also wonder why there is apparently no vestige of the independent scaling exponents, which has been observed for the moments of the voltage distribution on percolation clusters[35] and for the transit-time moments in a hierarchical model of the percolation backbone.[13] One important distinction is that these two situations are convective in nature, and higher moments are sensitive to an infinite set of distinct convective transport times. For dispersion on percolating networks, however, the higher moments are dominated by the diffusion time on the

TABLE I. Comparison of measured and predicted scaling exponents for a percolation lattice at very high $\hat{Q}$.

k	Measured exponent	Predicted exponent
1	−0.10	−0.11
2	0.76	0.75
3	1.6	1.61
4	2.6	2.47
5	3.4	3.33
6	4.2	4.19
7	5.0	5.05
8	5.8	5.91

longest dead ends, and the fine convective structure is unobservable.

E. Scaling of the percolation moments for arbitrary flow rates

To describe the transit-time data at general values of the velocity, we postulate a scaling form for the transit-time distribution. This form should interpolate between the two limiting behaviors given in Eqs. (77) and (78), in a manner that leads to a collapsing of the data for the moments at all values of $\hat{Q}$. One of the simplest ways that these limiting behaviors can be obtained within a scaling approach is if the transit-time distribution $P(t)$ has the form

$$P(t)=\frac{1}{t_D}F\left[\frac{t}{t_D},\frac{t_C}{t_D}\right], \tag{80}$$

with the scaling function F having the limiting behaviors

$$F(x,y)\rightarrow\begin{cases}F_1(x) & \text{as } y\rightarrow\infty\\ yF_2(x) & \text{as } y\rightarrow 0.\end{cases} \tag{81}$$

The zero-velocity limit corresponds to $y=\tau_C/\tau_D\rightarrow\infty$, in which case $\langle t^k\rangle\sim\tau_D^k$, while the convective limit corresponds to $y\rightarrow 0$, which leads to $\langle t^k\rangle\sim\tau_C\tau_D^{k-1}$. We hypothesize that the general form for $P(t)$ is given by Eq. (80). It then follows that the moments can be written in a scaled form

$$\frac{\langle t^k\rangle}{t_D^k}=\int_0^\infty dz\, z^k F\left[z,\frac{t_C}{t_D}\right]=G_k\left[\frac{t_C}{t_D}\right]. \tag{82}$$

In Figs. 15(a)–15(c) we have plotted our numerical data for the first three moments for values of $\hat{Q}=10^{-2}$, $10^{-1},\ldots,10^5$ and sizes $L=10,20,\ldots,70$ in the dimensionless form suggested in Eq. (82). Within our numerical precision, we find that the results for each moment indeed lie on unique scaling curves, and support the assertion that $P(t)$ has the simple scaling dependence given in Eq. (80).

VI. CONCLUSIONS

We have investigated the general problem of the transport of dynamically neutral tracer which is carried by fluid flow through a porous medium. Our primary focus has been on transport in random-network models of porous media, with emphasis on the behavior expected near the percolation threshold. In this kind of network, the background steady-state flow determines the ensuing motion of the tracer to be a locally biased continuum random-walk with the bias determined by the local flow velocity. This formulation allows us to account for the competition between convection (on the flowing fraction of the network) and diffusion (on dead ends and stagnant regions) in a meaningful fashion. This general approach represents what we believe to be a physically relevant generalization of the classical random walk on a percolation cluster to the case of finite flow rates and also to the continuum limit.

In the random networks that we studied, flow takes place on discrete links which are considered to be idealized one-dimensional tubes with no transverse degrees of freedom for the tracer. Furthermore, the tracer is assumed to mix completely at the tube junctions. These assumptions are only approximately correct in a typical porous medium, however. Under certain conditions, the first assumption may be eliminated altogether by replacing the molecular diffusion coefficient by the Taylor diffusion coefficient in a tube, as discussed in Sec. III. It is not evident how to improve upon the second assumption, and further work at the microscopic level is needed to resolve this issue. However, the degree of plausibility of these two assumptions is also coupled with the use of a

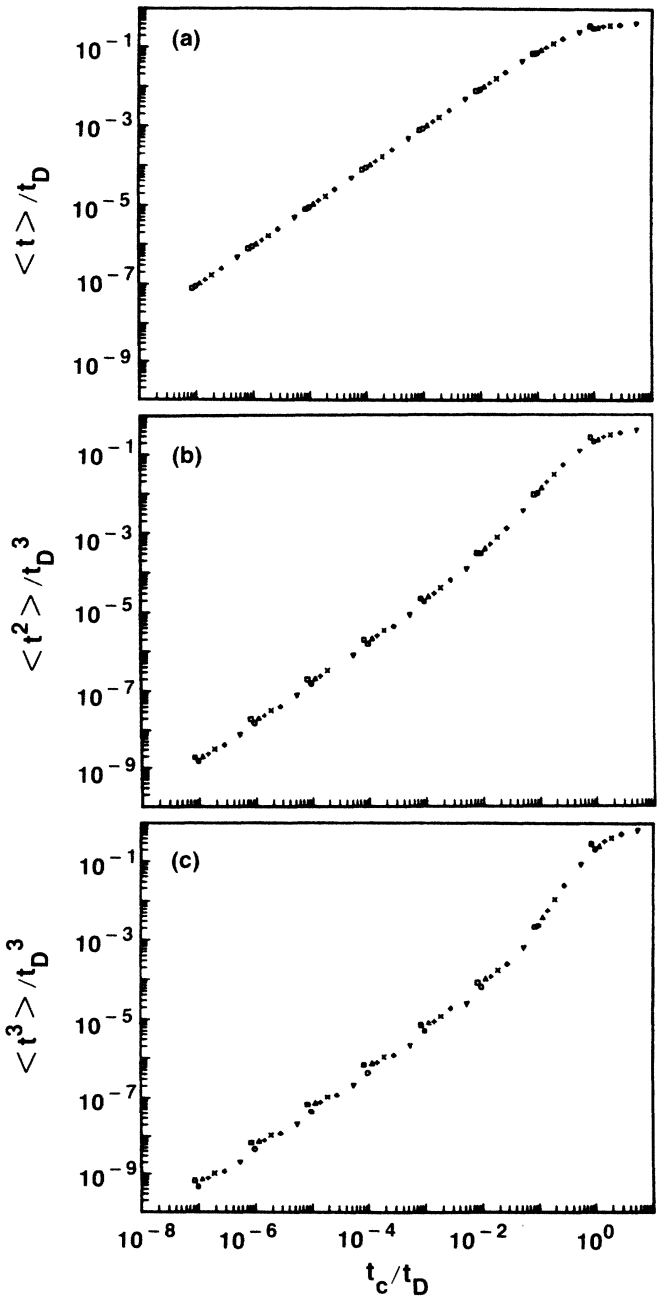

FIG. 15. Universal scaling of the moments for percolation lattices; (a) $k=1$, (b) $k=2$, (c) $k=3$.

percolation model to describe the medium. Our principal concern has been with cooperative effects on a scale of many pores, and one may therefore hope that the overall scaling behavior is insensitive to the local details of a specific model.

Within the percolation model, we have developed a computational approach which yields a formally exact solution for the transit-time distribution of the tracer, for arbitrary values of the fluid flow velocity. Several illustrative examples were solved in detail, from which we deduced the general behavior of the transit-time moments for percolation clusters. Furthermore, we have postulated a general scaling form for the transit-time distribution which leads to a unified account of the moments. Our numerical data on percolation clusters accord well with the intuition developed from the analytical study of small networks. As a particular case of the behavior of the moments, we have verified de Gennes's prediction for the variation of the macroscopic dispersivity with the correlation length.

Our ability to make progress on the problems considered here stems, to an important degree, from the fact that our model random medium is very well characterized. For percolation clusters, the statistical geometry of the medium is understood and the scaling exponents which determine its properties on long-length scales are known. However, the most striking physical examples of anomalous dispersion occur in geological situations, such as aquifers and petroleum reservoirs,[36] where the random medium is poorly characterized and its statistical properties are only partially understood. Even anomalous results in laboratory studies[37] are plagued by an incomplete knowledge of the geometry of the material. Percolation ideas do not seem immediately relevant to these situations, but we hope that some of our ideas, particularly the importance of studying the scaling behavior of the transit-time moments, will help in the general understanding of dispersion phenomena.

ACKNOWLEDGMENTS

We have benefited from very useful correspondence and discussions with a number of colleagues, including E. Charlaix, H. T. Davis, E. Guyon, E. J. Hinch, J.-P. Hulin, T. J. Plona, and M. Sahimi. The Center for Polymer Studies is supported in part by grants from the U.S. Army Research Office, the National Science Foundation, and the U.S. Office of Naval Research.

APPENDIX A: STATIC DIFFUSIVITY AND THE ELECTRICAL CONDUCTIVITY

We present two arguments for the relation (2) at Péclet number equal to zero, one quick and heuristic and the other more painstaking and rigorous.

Consider the Einstein relation for the electrical conductivity σ_0 of a fluid in terms of the density n of its charge carriers and their molecular diffusivity D_m,

$$\sigma_0=\frac{e^2}{kT}nD_m \ . \tag{83}$$

If we consider the analogous equation at the macroscopic level in the porous medium, then we have

$$\sigma=\frac{e^2}{kT}(n\phi)D_{\text{eff}} \ , \tag{84}$$

since the density of charge carriers is $n\phi$. Taking the quotient, we obtain the desired result

$$\frac{D_{\text{eff}}}{D_m}=\frac{\sigma}{\phi\sigma_0} \ . \tag{85}$$

Though oversimplified, this argument has the advantage that it clearly shows why the factor ϕ must center.

A more careful argument proceeds as follows. Imagine placing a small sphere of radius r and fixed tracer concentration ξ_0 within the pore space, and wait for a steady state to be established. Microscopically, the local tracer concentration $c(\mathbf{x})$ satisfies the *steady-state* diffusion equation and boundary conditions

$$\nabla^2 c=0, \quad c(|\mathbf{x}|=r)=\xi_0, \quad \hat{\mathbf{n}}\cdot\nabla c\,|_{\text{grain}}=0 \ . \tag{86}$$

The last condition is the assumption that tracer is not absorbed into the grains. The flux of tracer leaving an enveloping large sphere of radius R is

$$J_t(R)=-D_m\int_{|\mathbf{x}|=R} d\mathbf{S}\cdot\nabla_c \ . \tag{87}$$

Now consider the same problem from a macroscopic point of view, where there is a coarse-grained diffusivity D_{eff} and a concentration field $C(\mathbf{x})$, such that in steady state

$$\nabla^2 C=0, \quad C(|\mathbf{x}|=r)=\xi_0 \ . \tag{88}$$

At this level, the grains of the medium cannot be resolved, and there is no analog of the second boundary condition in Eq. (86). The macroscopic solution is just

$$C(\mathbf{x})=\frac{\xi_0 r}{|\mathbf{x}|} \ , \tag{89}$$

and the tracer flux leaving the outer sphere of radius R is

$$J_t(R)=4\pi\phi D_{\text{eff}}\xi_0 r \ . \tag{90}$$

The factor of ϕ appears because C is defined only within the pore space, so the surface area of the sphere is effectively $4\pi R^2\phi$.

Now consider an analogous electrical problem, where a conducting sphere of radius r and potential ξ_0 is in the pore space, so the governing equations for the potential are

$$\nabla^2 v=0, \quad v(|\mathbf{x}|=r)=\xi_0, \quad \hat{\mathbf{n}}\cdot\nabla v\,|_{\text{grain}}=0 \ , \tag{91}$$

and the current leaving the large sphere is

$$J_e(R)=-\sigma_0\int_{|\mathbf{x}|=R} d\mathbf{S}\cdot\nabla v \ . \tag{92}$$

Again, macroscopically, we have a potential field $V(\mathbf{x})$ and a conductivity σ such that

$$\nabla^2 V=0, \quad V(|\mathbf{x}|=r)=\xi_0 \ , \tag{93}$$

so that

$$V(\mathbf{x})=\frac{\xi_0 r}{|\mathbf{x}|} \ , \tag{94}$$

and the electrical flux leaving the large sphere is

$$J_e(R)=4\pi\sigma\xi_0 r \ . \tag{95}$$

(The macroscopic potential is defined over the entire porous medium so there is no factor of ϕ this time.) Now because the microscopic fields c and v satisfy the same differential equations and boundary conditions they are equal, and both surface integrals appearing above are identical. Eliminating the integral we obtain (2).

APPENDIX B: MATRIX INVERSION AND PROBABILITY PROPAGATION

The Laplace-transformed first-passage probability density $\tilde{P}(s)$ is given by

$$\tilde{P}(s)=\sum_j G_{Oj}^{-}\tilde{c}_j \ , \tag{96}$$

where the subscript O refers to the outlet node. The $\tilde{c}_i$ satisfy

$$\sum_j (G_{ij}^{+}\tilde{c}_i - G_{ij}^{-}\tilde{c}_j)=0 \tag{97}$$

for the interior nodes i, and

$$\sum_j (G_{Ij}^{+}\tilde{c}_I - G_{Ij}^{-}\tilde{c}_j)=1 \tag{98}$$

at the inlet node I. If we define a new quantity $\tilde{d}_i$ at each node by

$$\tilde{d}_i=\frac{\tilde{c}_i}{\sum_j G_{ij}^{+}} \ , \tag{99}$$

then Eqs. (96)–(98) become

$$\tilde{P}(s)=\sum_j p_{jO}\tilde{d}_j \ , \tag{100}$$

where

$$\tilde{d}_i=\sum_j p_{ji}\tilde{d}_j \tag{101}$$

for the interior nodes i, and

$$\tilde{d}_I=1+\sum_j p_{jI}\tilde{d}_j \ , \tag{102}$$

where the rescaled bond "conductances" p_{ji} are given by

$$p_{ji}=\frac{G_{ij}^{-}(m,s)}{\sum_k G_{jk}^{+}(m,s)} \tag{103}$$

$$=\frac{G_{ji}^{-}(-m,s)}{\sum_k G_{jk}^{+}(m,s)} \ . \tag{104}$$

Substituting for G^{+} and G^{-} their values given in (41) and (42), we find that the p_{ji} are precisely the quantities p_{ji} considered in Ref. 11. Furthermore, by working recursively through Eqs. (100)–(102), it is clear that the solution to (100) will be

$$\tilde{P}(s)=\sum_{\Gamma}\prod_{\text{links } ji} p_{ji} \ , \tag{105}$$

where the sum is over all distinct paths Γ from the inlet to the outlet which pass only once through the outlet (but may return to the inlet). In the high–Péclet-number limit, however, backflow paths do not contribute and the sum reduces to being only over distinct "downstream" paths. Formula (105) is the basis of the "probability propagation" algorithm developed in Ref. 11.

APPENDIX C: AVERAGE TIME AT HIGH PÉCLET NUMBER

At sufficiently large flow rate, the local Péclet number m in all the flowing links becomes large, and we can use the limiting forms of G^{+} and G^{-} given earlier in Sec. III to reduce the expression for the average transit time to a strikingly simple form. Let us expand the matrix equation for the $\tilde{c}_i$ in powers of s. To lowest order in s we have at node i

$$\sum_{j\,\text{out}} q_{ij}\tilde{c}_i^{(0)} - \sum_{j\,\text{in}} q_{ji}\tilde{c}_j^{(0)} + \sum_{j\,\text{dead}} g_{ij}(\tilde{c}_i^{(0)}-\tilde{c}_j^{(0)})=\delta_{iI} \ , \tag{106}$$

where the three sums denote the outgoing links, incoming links, and dead-end links, respectively. The inlet node has no incoming links, and for the internal nodes, we have, by flux conservation,

$$\sum_{j\,\text{out}} q_{ij}=\sum_{j\,\text{in}} q_{ji} \ . \tag{107}$$

Thus the above reduce to

$$\sum_{j\,\text{in}} q_{ji}(\tilde{c}_i^{(0)}-\tilde{c}_j^{(0)}) + \sum_{j\,\text{dead}} g_{ij}(\tilde{c}_i^{(0)}-\tilde{c}_j^{(0)})=0 \tag{108}$$

for the internal nodes i, and

$$\sum_{j\,\text{out}} q_{Ij}\tilde{c}_I^{(0)} + \sum_{j\,\text{dead}} g_{Ij}(\tilde{c}_I^{(0)}-\tilde{c}_j^{(0)})=1 \tag{109}$$

at the inlet node I. By inspection, the solution to this is that the $\tilde{c}_i^{(0)}$ are all equal,

$$\tilde{c}_i^{(0)}=\frac{1}{Q} \ , \tag{110}$$

where

$$Q=\sum_{j\,\text{out}} q_{Ij} \tag{111}$$

is the total flux entering the network. To first order in s we have

$$\sum_{j\,\text{out}} q_{ij}\tilde{c}_i^{(1)} - \sum_{j\,\text{in}} q_{ji}\tilde{c}_j^{(1)} + \sum_{j\,\text{dead}} g_{ij}(\tilde{c}_i^{(1)}-\tilde{c}_j^{(1)}) + \sum_{j\,\text{in}} V_{ij}\tilde{c}_j^{(0)} + \sum_{j\,\text{dead}} V_{ij}\left[\frac{\tilde{c}_i^{(0)}}{3}+\frac{\tilde{c}_j^{(0)}}{6}\right]=0 \tag{112}$$

for the internal nodes i, and

$$\sum_{j\,\text{out}} q_{Ij}\tilde{c}_I^{(1)} + \sum_{j\,\text{dead}} g_{Ij}(\tilde{c}_I^{(1)}-\tilde{c}_j^{(1)}) + \sum_{j\,\text{dead}} V_{Ij}\left[\frac{\tilde{c}_I^{(0)}}{3}+\frac{\tilde{c}_j^{(0)}}{6}\right]=0 \tag{113}$$

at the inlet node I. The outlet node equation reads

$$-\sum_{j \text{ in}} q_{jO}\tilde{c}_j^{(1)}+\sum_{j \text{ in}} V_{Oj}\left[\frac{\tilde{c}_i^{(0)}}{3}+\frac{\tilde{c}_j^{(0)}}{6}\right]=\langle t\rangle \ , \quad (114)$$

where $\langle t\rangle$ is the desired average time to cross the network (recall that there are no dead-end nodes attached to the outlet). If we sum these equations over all the nodes (including the inlet and outlet), then the terms involving the $\tilde{c}_i^{(1)}$ all cancel, and we obtain [using the zeroth-order solution (110)]

$$\langle t\rangle=\sum_{\text{flowing}}\frac{V_{ij}}{Q}+2\sum_{\text{dead}}\frac{V_{ij}}{2Q}=\frac{V}{Q} \ , \quad (115)$$

where V is the total volume of the network.

APPENDIX D: PHYSICAL UNITS AND THE COMPUTER SIMULATION

In our numerical calculations on the $n_x \times n_y$ lattice shown in Fig. 3, we first assign unit flow conductance to each bond ij, a unit pressure drop across the system, and compute the node pressures $\hat{p}_i$, from which we determine bond fluxes $\hat{q}_{ij}=\hat{p}_i-\hat{p}_j$ and a total flux $\hat{Q}_0$ entering and leaving the network.

First we note that $\hat{Q}_0$ is trivially related to the effective conductivity of the network. We imagine that the bonds are identical cylinders of radius r and length l, and that the solid surrounding the fluid is a block of dimensions $n_x l \times n_y l \times l$. (Note that we here consider a set of three-dimensional cylinders connected in a two-dimensional square lattice; we could also discuss a two-dimensional "etched" pattern, but this would merely change some of the numerical constants in this appendix.) The electrical conductance of each cylinder is then $\sigma_0 \pi r^2/l$, and the total current flowing is just this factor times $\hat{Q}_0$. The effective conductivity is the current density per unit potential gradient, which is the total current per unit cross-sectional area $n_y l \times l$, divided by the (unit) voltage drop over the system length $n_x l$, which yields

$$\sigma=\frac{\sigma_0 \pi r^2}{l^2}\frac{n_x}{n_y}\hat{Q}_0 \ . \quad (116)$$

Similarly, the porosity ϕ is the volume per cylinder times the number of bonds N_B divided by the system volume, or

$$\phi=\frac{\pi r^2}{l^2}\frac{N_B}{n_x n_y} \ , \quad (117)$$

so that the combination appearing in Eq. (2) is

$$\frac{\sigma}{\sigma_0 \phi}=\frac{n_x^2}{N_B}\hat{Q}_0 \ . \quad (118)$$

To consider the dispersion problem in physical terms, we suppose that the fluid has viscosity μ, and the net pressure drop is ΔP, so that the physical flow conductance (for Poiseuille flow) is $\pi r^4/8\mu l$, the resulting pressures are $\Delta P \cdot \hat{p}_i$, and the physical single-bond and total fluxes are $\pi r^4 \Delta P/8\mu l$ times $\hat{q}_{ij}$ and $\hat{Q}_0$, respectively. It is convenient to write the pressure in the form

$$\Delta P=\lambda\frac{16\mu D_m}{r^2} \ , \quad (119)$$

where λ is dimensionless, because then the single-bond Péclet number is

$$m_{ij}=\frac{q_{ij}}{\pi r^2}\frac{l}{2D_m}=\lambda \hat{q}_{ij} \ . \quad (120)$$

Furthermore, the total flux is

$$Q=\frac{2\pi r^2 D_m}{l}\lambda \hat{Q}_0 \ , \quad (121)$$

and we identify $\hat{Q}=\lambda \hat{Q}_0$ as the dimensionless control variable in the numerical simulations. Some physical feeling for λ is obtained by considering a fully occupied lattice, where $\hat{Q}_0=n_y/n_x$, and it follows that

$$\lambda=\frac{(Q/2\pi r^2 n_y)(ln_x)}{D_m}=\frac{UL}{D_m} \ . \quad (122)$$

Here U is the average fluid velocity and L the system length so λ is twice the Péclet number introduced in Eq. (1).

[1] J. Bear, *Dynamics of Fluids in Porous Media* (Elsevier, Amsterdam, 1971).

[2] J. J. Fried and M. A. Combarnous, Adv. Hydros. **7**, 169 (1971).

[3] A. E. Scheidegger, *The Physics of Flow in Porous Media*, 3rd ed. (University of Toronto, Toronto, 1974).

[4] M. Sahimi, H. T. Davis, and L. E. Scriven, Chem. Eng. Commun. **23**, 329 (1983).

[5] M. Sahimi, A. L. Heiba, B. D. Hughes, L. E. Scriven, and H. T. Davis, Chem. Eng. Sci. **41**, 2103 (1986); **41**, 2123 (1986).

[6] D. L. Koch and J. F. Brady, J. Fluid Mech. **154**, 399 (1985).

[7] D. Stauffer, *Introduction to Percolation Theory* (Taylor and Francis, London, 1985).

[8] P. G. de Gennes and E. Guyon, J. Mec. **17**, 403 (1978).

[9] R. Lenormand and S. Bories, C. R. Acad. Sci. Ser. B **291**, 279 (1980); R. Lenormand, in *Physics and Chemistry of Porous Media II*, edited by J. R. Banavar, J. Koplik, and K. W. Winkler (AIP, New York, 1987).

[10] R. Chandler, J. Koplik, K. Lerman, and J. Willemsen, J. Fluid Mech. **119**, 249 (1982); D. Wilkinson and J. Willemsen, J. Phys. A **16**, 3365 (1983); D. Wilkinson, Phys. Rev. A **34**, 1380 (1986).

[11] L. de Arcangelis, J. Koplik, S. Redner, and D. Wilkinson, Phys. Rev. Lett. **57**, 996 (1986).

[12] See also M. Leitzlement, P. Maj, J. A. Dodds, and J. L. Greffe, in *Solid-Liquid Separation*, edited by J. Gregory (Ellis Horwood, Chichester, England, 1984).

[13] S. Redner, J. Koplik, and D. Wilkinson, J. Phys. A **20**, 1543 (1987).

[14]Y. Gefen, A. Alexander, and A. Aharony, Phys. Rev. Lett. **50**, 77 (1982).

[15]G. I. Taylor, Proc. R. Soc. London, Ser. A **219**, 186 (1953).

[16]See also R. Aris, Proc. R. Soc. London, Ser. A **235**, 67 (1956).

[17]P. G. de Gennes, J. Fluid Mech. **136**, 189 (1983).

[18]G. de Josselin de Jong, Trans. Am. Geophys. Union **39**, 67 (1958).

[19]P. G. Saffman, J. Fluid Mech **6**, 321 (1959); **7**, 194 (1960).

[20]J.-C. Bacri, N. Rokotomalala, and D. Salin, Phys. Rev. Lett. **58**, 2035 (1987).

[21]Taylor (Ref. 15) and Aris (Ref. 16) derived the dispersion coefficient for laminar flow in a long cylindrical tube of radius r as $D_{\parallel}=D_m+U^2r^2/48D_m$. This velocity-dependent term may be understood from the random-walk point of view of this section as follows. Consider a reference frame moving with the average fluid velocity; the tracer can be thought of as making random diffusive jumps between the forward-moving region near the center of the pipe to the backward-moving region near the walls. The step length is again $l\sim U\tau$, while the step time is now the molecular diffusion time across the pipe, $\tau\sim r^2/D_m$, where r is the pipe radius. Thus $D_{\parallel}\sim l^2/\tau\sim U^2r^2/D_m$.

[22]K. H. Coats and B. D. Smith, Soc. Petrol. Eng. J. **4**, 73 (1964).

[23]See, e.g., G. Michel, J. Phys. A **19**, 2461 (1986); A. Bunde, S. Havlin, H. E. Stanley, B. Trus, and G. H. Weiss, Phys. Rev. B **34**, 8129 (1986).

[24]I. Goldhirsch and Y. Gefen, Phys. Rev. A **33**, 2583 (1986); S. H. Noskowicz and I. Goldhirsch (unpublished).

[25]See, e.g., D. Ben-Avraham and S. Havlin, J. Phys. A **15**, L691 (1982); (unpublished), and extensive references therein.

[26]M. Barma and D. Dhar, J. Phys. C **16**, 1451 (1983).

[27]S. Roux, C. Mitescu, E. Charlaix, and C. Baudet, J. Phys. A **19**, L687 (1986).

[28]R. Mann, P. N. Sharratt, and G. Thompson, Chem. Eng. Sci. **41**, 711 (1986).

[29]M. Sahimi and A. O. Imdakm (unpublished).

[30]R. Aris, Chem. Eng. Sci. **11**, 194 (1959).

[31]E. B. Nauman and B. A. Buffham, *Mixing in Continuous Flow Systems* (Wiley, New York, 1983).

[32]J. W. Essam, in *Phase Transitions and Critical Phenomena*, edited by C. Domb and M. S. Green (Academic, New York, 1972), Vol. 2.

[33]H. Stehfest, Commun. ACM **13**, 47 (1970).

[34]J. Vannimenus, J. Phys. Lett. **45**, L1071 (1984).

[35]L. de Arcangelis, S. Redner, and A. Coniglio, Phys. Rev. B **31**, 4725 (1985); **34**, 4656 (1986); R. Rammal, C. Tannous, and A.-M. S. Tremblay, Phys. Rev. Lett. **54**, 1718 (1985); B. Fourcade, P. Breton, and A.-M. S. Tremblay (unpublished).

[36]G. Dagan, Ann. Rev. Fluid Mech. **19**, 183 (1987), and earlier references therein.

[37]E. Charlaix, J.-P. Hulin, and T. J. Plona, Phys. Fluids **30**, 1690 (1987).